

Bacterial Iron Transport: Coordination Properties of Pyoverdin PaA, a Peptidic Siderophore of *Pseudomonas aeruginosa*

Anne-Marie Albrecht-Gary,^{*,†} Sylvie Blanc,[†] Natacha Rochel,[†] Aydin Z. Ocaktan,[‡] and Mohamed A. Abdallah[‡]

Laboratoire de Physico-Chimie Bioinorganique, URA 405 CNRS, EHICS, 1 rue Blaise Pascal, 67000 Strasbourg, France, and Laboratoire de Chimie Microbienne, URA 31 CNRS, Faculté de Chimie, 1 rue Blaise Pascal, 67000 Strasbourg, France

Received August 11, 1994[⊗]

Pyoverdin PaA is a siderophore excreted by *Pseudomonas aeruginosa*, a common and pathogenic bacterium. It belongs to a family of fluorescent iron(III) biological ligands. Its chemical structure shows three bidentate coordination sites, two hydroxamic acids and a dihydroxyquinoline-type function bound to a peptidic chain. Spectrophotometric, potentiometric and cyclic voltammetric measurements allowed the determination of the acid–base functions of the free siderophore as well as the iron(III) and iron(II) coordination properties. Pyoverdin PaA forms neutral and strong ferric complexes at physiological pH. The thermodynamic stability of its ferric and ferrous complexes is very similar to that of linear trihydroxamate siderophores, such as ferrioxamine B (Desferal) and coprogen, in spite of its anchored structure and of a catechol-type binding site. As for trihydroxamate ligands, the reduction potential was found to be accessible to physiological reductant systems and an iron(III) release mechanism via a reduction step could be proposed. Kinetic studies carried out by either classical or stopped-flow spectrophotometry have provided the kinetic parameters related to the formation and the dissociation of the ferric pyoverdin PaA complexes in acidic conditions. Stepwise mechanisms revealed the flexibility of this strong ligand. The binding of the terminal hydroxamic acid of pyoverdin PaA is proposed to be the rate limiting step of the iron(III) coordination process. The dissociation mechanism showed an unfolding of the siderophore leading to protonated ferric intermediate species corresponding to the successive protonation of the binding sites. Accessible reduction potential to physiological reductants, fast iron(III) uptake kinetics and efficient assistance of the protons to the iron(III) release mechanism are favorable features for iron biological transport by pyoverdin PaA.

Introduction

Siderophores are small molecules (MW ca. 400–2000 Da), produced in iron deficient conditions by microorganisms, that bind and facilitate the transport of external iron into the cells via a high affinity system.^{1,2} They generally possess three bidentate chelating groups which can be either three catechol groups^{3,4} or three hydroxamate groups^{5,6} or miscellaneous groups.^{7,8}

The most studied natural compounds are enterobactin,³ and agrobactin⁴ which contain three catechol groups. Another group of widespread fungal or bacterial siderophores are the linear or cyclic trihydroxamates such as ferrichromes,⁶ coprogens,⁹ ferrioxamines⁵ and some fusarinines.¹⁰ Other siderophores produced by various microorganisms possess both hydroxamate

and hydroxyacid or other less common chelating groups. The three bidentate groups can be either two hydroxamates and one hydroxyphenyloxazolin group as in the mycobactins,¹¹ two catechols and one hydroxyphenyloxazolin group as in parabactin,¹² two hydroxamates and one hydroxyacid group as in aerobactin,¹³ or two amino acid groups and one hydroxyacid group as in mugineic acid,¹⁴ a phytosiderophore.

Many trihydroxamate^{15–18} or tricatecholate^{19–22} analogues have been synthesized in order to determine the most important structural features for strong iron binding and molecular recognition by membrane receptors. These synthetic ligands are chelating agents that may be potentially useful in iron overload which occurs in widespread genetic diseases, like

[†] EHICS.

[‡] Faculté de Chimie.

[⊗] Abstract published in *Advance ACS Abstracts*, November 1, 1994.

- (1) Neilands, J. B. *Struct. Bonding* **1984**, *58*, 1–25.
- (2) Raymond, K. N.; Müller, G.; Matzanke, B. F. *Top. Curr. Chem.* **1984**, *123*, 49–102. Winkelmann, G. In *Handbook of Microbial Iron Chelates*; Winkelmann, G., Ed.; CRC Press: Boca Raton, FL 1991; pp 15–64.
- (3) O'Brien, G.; Gibson, F. *Biochim. Biophys. Acta* **1976**, *215*, 393–402.
- (4) Eng-Wilmot, D. L.; Van Der Helm, D. *J. Am. Chem. Soc.* **1980**, *102*, 7719–7725.
- (5) Bickel, H.; Hall, G. E.; Keller-Schierlein, W.; Prelog, V.; Vischer, E.; Wettstein, A. *Helv. Chim. Acta* **1960**, *43*, 2129–2138.
- (6) Neilands, J. B. *J. Am. Chem. Soc.* **1952**, *74*, 4846–4847.
- (7) Hider, R. C. *Struct. Bonding* **1984**, *58*, 25–88.
- (8) Teintze, M.; Hossain, M. B.; Barnes, C. L.; Leong, J.; Van Der Helm, D. *Biochemistry* **1981**, *20*, 6446–6457.
- (9) Keller-Schierlein, W.; Diekmann, H. *Helv. Chim. Acta* **1970**, *53*, 2035–2044.
- (10) Sayer, J. M.; Emery, T. *Biochemistry* **1968**, *7*, 184–190.
- (11) Snow, G. A. *J. Chem. Soc.* **1954**, 4080–4093.
- (12) Tait, G. H. *Biochem. J.* **1975**, *146*, 191–204.
- (13) Harris, W. R.; Carrano, C. J.; Raymond, K. N. *J. Am. Chem. Soc.* **1979**, *101*, 2722–2727.
- (14) Sugiura, Y.; Tanaka, H.; Mino, Y.; Ishida, T.; Ota, N.; Inoue, M.; Nomoto, K.; Yoshioka, H.; Takemoto, T. *J. Am. Chem. Soc.* **1981**, *103*, 6979–6982.
- (15) Sun, Y.; Martell, A. E.; Motekaitis, R. J. *Inorg. Chem.* **1985**, *24*, 4343–4350.
- (16) Shanzer, A.; Libman, J.; Lazar, R.; Tor, Y. *Pure Appl. Chem.* **1989**, *61*, 1529–1534.
- (17) Ng, C. Y.; Rodgers, S. J.; Raymond, K. N. *Inorg. Chem.* **1989**, *28*, 2062–2066.
- (18) Yakirevitch, P.; Rochel, N.; Albrecht-Gary, A. M.; Libman, J.; Shanzer, A. *Inorg. Chem.* **1993**, *32*, 1779–1787.
- (19) Harris, W. R.; Raymond, K. N. *J. Am. Chem. Soc.* **1979**, *101*, 6534–6541.
- (20) Stack, T. D. P.; Hou, Z.; Raymond, K. N. *J. Am. Chem. Soc.* **1993**, *115*, 6466–6467.
- (21) Rodgers, S. J.; Lee, C. W.; Ng, C. Y.; Raymond, K. N. *Inorg. Chem.* **1987**, *26*, 1622–1625.
- (22) Tor, Y.; Libman, J.; Shanzer, A.; Felder, C. E.; Lifson, S. J. *J. Am. Chem. Soc.* **1992**, *114*, 6661–6671.

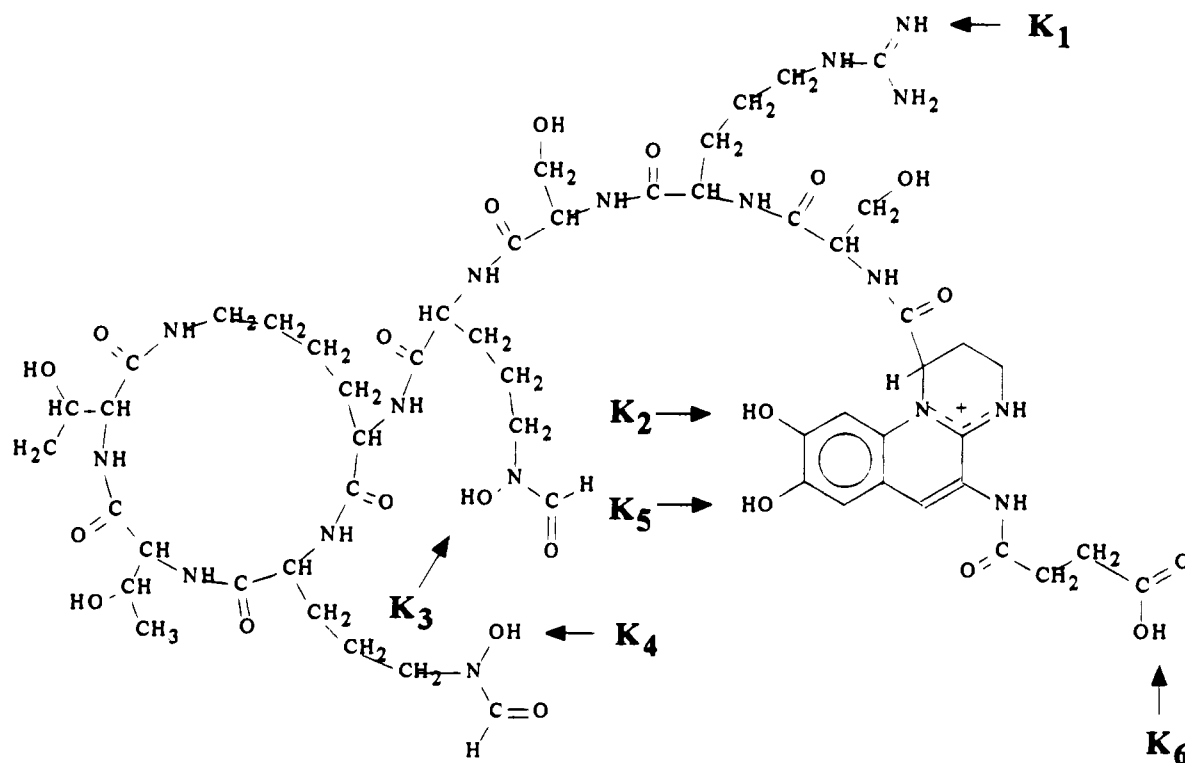


Figure 1. Structure of the fully protonated form of pyoverdine PaA.

β -thalassemia²³ or hemochromatosis.²⁴ Recently, ferrioxamine B catechol derivatives,²⁵ macrobicyclic analogues^{26–29} and iron(III) helicates^{30,31} have been synthesized.

Among the miscellaneous bacterial siderophores, pyoverdins^{32–35} form a special class, since they are produced by most of the fluorescent *Pseudomonas* and show many structural similarities.

Under iron-deficient conditions, *Pseudomonas aeruginosa* excretes three fluorescent peptidic siderophores, pyoverdins Pa, PaA and PaB. *P. aeruginosa* is a common pathogenic bacterium which causes 10–20% of the infections in hospitals.³⁶ The virulence of *P. aeruginosa* is closely related to its iron metabolism.³⁷ The structure of these pyoverdins has been elucidated in absence of crystals, using FAB mass spectrometry

and NMR techniques.^{38,39} These hydrosoluble compounds show very similar structures consisting of a peptide chain bound by its N-terminus to a chromophore derived from 2,3-diamino-6,7-dihydroxyquinoline. They only differ by an acyl substituent bound to the C-3 of the chromophore. They form iron(III) complexes by means of three bidentate chelating groups including a catechol, a hydroxamate at the end of the peptide chain and a second hydroxamate function in the middle of the peptide chain. Figure 1 shows the structure of pyoverdine PaA.

The coordination properties are important in understanding biological iron transport by pyoverdine siderophores. In order to assess the physiological role of pyoverdine PaA, its affinity for ferric ion and the mechanisms of iron complexation and release, we present in this article the complete results of the electrochemical, potentiometric, spectrophotometric and kinetic studies of pyoverdine PaA and its iron complexes.

Experimental Section

Preparation and Purification of Pyoverdine PaA and Its Ferric Species. Pyoverdine PaA was isolated and purified from cultures of *P. aeruginosa* ATCC 15692 (PAO1) according to a published procedure³⁸ with some modifications.

Growth Conditions. The strain was grown aerobically at 25 °C in conical flasks containing 0.5 L of culture medium and subject to mechanical agitation. The culture medium used had the following composition per liter: K₂HPO₄, 6.0 g; KH₂PO₄, 3.0 g; (NH₄)₂SO₄, 1.0 g; MgSO₄·7H₂O, 0.2 g; succinic acid, 4.0 g. It was adjusted to p[H⁺] 7.0 before sterilization. To reduce iron contamination, deionized, distilled water was used, and glassware was carefully prewashed with acid and rinsed with distilled water before use.

Isolation and Purification of the Pyoverdins. After 48 h, the culture medium (4.5 L overall) was centrifuged (20 000 g for 30 min at 4 °C), acidified to p[H⁺] 4.0 by careful addition of formic acid, ultrafiltered through a 0.45 μ m membrane (Minitan, Millipore, Molsheim,

- (23) Crichton, R. R. *Inorganic Biochemistry of Iron Metabolism*; Ellis Horwood: London, 1991; Chapter 10, pp 183–186.
 (24) Weinberg, E. D. *Quart. Rev. Biol.* **1989**, *64*, 261–290.
 (25) Hou, Z.; Whisenhunt, D. W.; Xu, J., Jr.; Raymond, K. N. *J. Am. Chem. Soc.* **1994**, *116*, 840–846.
 (26) Seel, C.; Vögtle, F. *Angew. Chem., Int. Ed. Engl.* **1992**, *31*, 528–549.
 (27) Garrett, T. M.; McMurry, T. J.; Hosseini, M. W.; Reyes, Z. E.; Hahn, F. E.; Raymond, K. N. *J. Am. Chem. Soc.* **1991**, *113*, 2965–2977.
 (28) Pierre, J. L.; Baret, P.; Gellon, G. *Angew. Chem., Int. Ed. Engl.* **1991**, *30*, 85–86.
 (29) Sun, Y.; Martell, E. *Tetrahedron* **1990**, *46*, 2725–2736.
 (30) Libman, J.; Tor, Y.; Shanzer, A. *J. Am. Chem. Soc.* **1987**, *109*, 5880–5881.
 (31) Tor, Y.; Libman, J.; Shanzer, A. *J. Am. Chem. Soc.* **1987**, *109*, 6518–6519.
 (32) Abdallah, M. A. In *Microbial Iron Chelates*; Winkelmann, G., Ed.; CRC Press Inc.: Boca Raton, FL, 1991; pp 139–153.
 (33) Geisen, K.; Taraz, K.; Budzikiewicz, H. *Monatsh. Chem.* **1992**, *123*, 151–178.
 (34) Buyer, J. S.; Kratzke, M. G.; Sikora, L. *J. Appl. Environ. Microbiol.* **1993**, *59*, 677–681.
 (35) Linget, C.; Azadi, P.; MacLeod, J. K.; Dell, A.; Abdallah, M. A. *Tetrahedron Lett.* **1992**, *33*, 1737–1740.
 (36) Doggett, R. G. In *Pseudomonas aeruginosa: Clinical Manifestations of Infection and Current Therapy*; Academic Press: New York, 1979; pp 1–494.
 (37) Ankenbauer, R.; Sriyosachati, S.; Cox, C. D. *Infect. Immun.* **1985**, *49*, 132–140.

- (38) Demange, P.; Wendenbaum, S.; Linget, C.; Mertz, C.; Cung, M. T.; Dell, A.; Abdallah, M. A. *Biol. Met.* **1990**, *3*, 155–170.
 (39) Briskot, G.; Taraz, K.; Budzikiewicz, H. *Liebigs Ann. Chem.* **1989**, 375–384.

France), and applied to a column ($l = 20$ cm; $\Phi = 25$ mm) of octadecylsilane (Lichroprep RP 18, 40–63 μm , Merck, Darmstadt). The column was first washed with an aqueous solution of acetic acid at $p[\text{H}^+] 4.0$ (0.5 L), in order to remove the bulk of inorganic salts and then the crude siderophores were eluted with a 1:1 mixture of acetonitrile/0.05 M pyridine–acetic acid buffer $p[\text{H}^+] 5.0$ (0.5 L). After evaporation, the mixture of pyoverdins was dissolved in pyridine–acetic acid buffer and applied to a CM-Sephadex C-25 ion-exchange column ($l = 30$ cm, $\Phi = 35$ mm) prepared in the same buffer. The column was first eluted isocratically with 0.05 M pyridine–acetic acid buffer $p[\text{H}^+] 5.0$ (0.6 L), then with a linear gradient of the same buffer (0.05–2 M; 2×1 L). The fractions (5 mL) were monitored by spectrophotometry at 380 nm, combined and evaporated. Three main siderophores were isolated at this stage: pyoverdin PaB (150 mg), pyoverdin PaA (350 mg, the major compound) and pyoverdin Pa (200 mg).

Each pyoverdin was dissolved in water (5 mL), treated with 5 equiv of a 2 M ferric chloride solution, filtered first over an octadecylsilane column (eluted as above) in order to remove excess iron salts and then on a CM-Sephadex C-25 ion-exchange column eluted isocratically with pyridine–acetic acid buffer. This chromatography was monitored spectrophotometrically at 403 nm. Each of the pyoverdin Pa, PaA and PaB iron(III) complexes, obtained after CM-Sephadex column chromatography, was found to be a single major compound after reverse phase HPLC. Although analytical HPLC and electrophoresis showed the compounds to be fairly pure, the fractions containing pyoverdin PaA ferric complex were combined, lyophilized and applied to a preparative HPLC (10 μm particle size C-18 nucleosil from Macherey-Nagel as the bonded phase, $l = 25$ cm, $\Phi = 25$ mm). This step appeared to be crucial for further structural and physicochemical determination on pyoverdins, and may be of importance in biochemical or biological assays involving these siderophores, since cyclic voltammograms performed on various samples at this stage showed the presence of an irreversible redox step due to impurities which were discarded during this preparative HPLC treatment.

Preparation of Iron-Free Pyoverdin PaA. In order to overcome the rather tedious aspects of the former procedure using 8-hydroxyquinoline to remove iron(III) from pyoverdin,⁴⁰ another procedure was devised using EDTA as a competitor iron(III) chelate: 150 mg of HPLC purified pyoverdin PaA ferric complex were dissolved in 3 mL water at $p[\text{H}^+] 4.0$ and 10 mL of a 0.2 M EDTA solution added. The solution was stirred for one hour, diluted twice with water at $p[\text{H}^+] 4.0$ and purified by chromatography over an ODS reverse phase column ($l = 15$ cm; $\Phi = 20$ mm). The column was first washed with 50 mL of a 0.1 M EDTA solution, then with 400 mL water at $p[\text{H}^+] 4.0$. Pyoverdin PaA was recovered as a free ligand after elution with a linear gradient of water $p[\text{H}^+] 4.0$ –20% methanol in water $p[\text{H}^+] 4.0$.

Iron-free pyoverdin PaA was lyophilized, resuspended in 0.05 M pyridine–acetic acid, applied to a CM-Sephadex C25 ion exchange column and eluted with a gradient of 0.05–1 M pyridine–acetic acid $p[\text{H}^+] 5.0$ to remove any traces of metallated pyoverdin and EDTA from the purified pyoverdin.

Criteria of Purity. The criteria used to check the purity of pyoverdins and their complexes are film electrophoresis, HPLC and cyclic voltammetry. The last method was found to be very sensitive and very useful for preparative work.

Electrophoretic analyses were performed on cellulose acetate sheets at 300 V, over a period of 30 min; in 0.1 M pyridine–acetic acid buffer, $p[\text{H}^+] 5.0$. The pyoverdins and their iron complexes migrate to the cathode. The migration distances were respectively 3 mm, 6 mm and 15 mm for pyoverdin PaB, pyoverdin PaA and pyoverdin Pa ferric complexes, and 8 mm, 15 mm and 24 mm for the corresponding free ligands. On excitation at 365 nm, the free ligands presented a yellowish fluorescence whereas the iron complexes were non-fluorescent.

HPLC analyses of the free ligands required the pretreatment of the columns by EDTA solutions to remove any trace of metallic cations which are a main source of interference for these types of compounds.⁴¹

The eluent system which contains EDTA and octylsulfonic acid allows a very efficient and reproducible separation of pyoverdins by ion pair liquid chromatography in the presence of octylsulfonic acid.⁴²

Iron-free pyoverdin PaA was analyzed by analytical HPLC using a column (0.5 cm \times 26 cm) containing ODS (5 μm particle size: Supelco). Samples were eluted with a buffer containing citric acid (0.2 M), 1.0 mM EDTA, 1 mM 1-octane sulfonic acid, Na_2HPO_4 (0.2 M), and 10% (v/v) acetonitrile at $p[\text{H}^+] 3.0$. Elution of iron-free pyoverdin was monitored with a spectrophotometer at a wavelength of 380 nm. The retention times were 3.7 min, 10.0 min, and 8.7 min, respectively, for pyoverdin PaB, pyoverdin PaA and pyoverdin Pa.

Potentiometric and Spectrophotometric Experiments. The solutions were prepared with deionized water and the ionic strength was fixed, using 0.1 M sodium perchlorate (MERCK, p.a.). Purified and characterized solid samples of the free pyoverdin PaA and its ferric species were dissolved and introduced into a jacketed cell (25 mL) maintained at 25.0 ± 0.1 °C by the flow of a HAAKE FJ thermostat. The concentrations were calculated using the extinction coefficients⁴³ $\epsilon_{403} = 19\,000 \text{ M}^{-1} \text{ cm}^{-1}$, $\epsilon_{460} = 6500 \text{ M}^{-1} \text{ cm}^{-1}$ and $\epsilon_{540} = 3500 \text{ M}^{-1} \text{ cm}^{-1}$ for the ferric complex and $\epsilon_{364} = 16\,000 \text{ M}^{-1} \text{ cm}^{-1}$ and $\epsilon_{380} = 16\,500 \text{ M}^{-1} \text{ cm}^{-1}$ for the free pyoverdin PaA at $p[\text{H}^+] = 5.0$. The solutions were deoxygenated and continuously flushed with Argon during the titrations, in order to prevent oxidation⁷ of the catechol moiety of pyoverdin PaA. Simultaneous $p[\text{H}^+]$ and UV–visible spectrophotometric measurements (250–600 nm) were carried out. The free hydrogen concentrations were measured with an Ag/AgCl combined glass electrode (TACUSSEL, High Alkalinity, saturated sodium chloride) and a TACUSSEL ISIS 20 000 millivoltmeter. Standardization of the millivoltmeter and verification of the linearity ($3 < p[\text{H}^+] < 9$) of the electrode were performed using commercial buffers (MERCK, Titrisol) according to classical methods.⁴⁴ The titration of the free siderophore (10^{-4} M, $1.7 < p[\text{H}^+] < 13.0$) and of its iron(III) species (10^{-4} M, $1.2 < p[\text{H}^+] < 9.0$) was carried out by addition of known volumes of either sodium hydroxide (0.1 M, MERCK, Titrisol) or hydrochloric acid (0.1 M, MERCK, Titrisol) with a MANOSTAT microburet. For the acid–base titration of the pyoverdin ferric species, special care was taken to ensure that complete equilibration was attained, that the potentiometric and spectrophotometric measurements were stable over a period of several hours. When equilibrium conditions were reached, absorption spectra were run on small samples (0.5 mL). The spectrophotometric measurements were recorded using a KONTRON UVIKON 860 spectrophotometer and HELLMA quartz optical cells (0.2 cm). An example of the spectral evolution of free pyoverdin PaA and of its ferric species as a function of hydrogen ion concentrations is given in Figure 2.

Potentiometric data obtained during the titration of free pyoverdin PaA were processed with the MINQUAD program⁴⁵ using an iterative least-squares Marquardt refinement. The simultaneous potentiometric and spectrophotometric data recorded at various $p[\text{H}^+]$ values for pyoverdin PaA in the presence or absence of iron(III) were fitted with the LETAGROP-SPEFO program.⁴⁶ This program uses a Raphson-Newton algorithm and a pit-mapping method and calculates the thermodynamic constants of the absorbing species and their corresponding electronic spectra.

Electrochemistry. Cyclic voltammetric measurements were made on a TACUSSEL GSTP instrument and a TACUSSEL PRG5 potentiostat. Voltammograms were obtained either with a TEKTRONIX oscilloscope or a SEFRAM X-Y recorder. A dropping mercury electrode was used as the working electrode, a Pt wire as a counter electrode and a saturated sodium chloride calomel electrode (SCE) as a reference electrode in a jacketed cell (5 mL, METROHM) maintained at 25.0 ± 0.1 °C (HAAKE FJ thermostat). The supporting electrolyte

(40) Meyer, J. M.; Abdallah, M. A. *J. Gen. Microbiol.* **1978**, *107*, 319–328.

(41) Cramer, S. M.; Nathanael, B.; Horvath, C. *J. Chromatogr.* **1984**, *295*, 405–411.

(42) Knox, J. H. *High Performance Liquid Chromatography*; Edinburgh University Press, Edinburgh, U.K., 1978; pp 52–59.

(43) Demange, P.; Wendenbaum, S.; Bateman, A.; Dell, A.; Abdallah, M. A. In *Iron Transport in Microbes, Plants and Animals*; Winkelmann, G., Ed.; Van der Helm, D., Neilands, J. B., Eds.; VCH: Weinheim, Germany, 1987; Chapter 10, pp 167–187.

(44) Martell, A. E.; Motekaitis, R. J. *Determination and Use of Stability Constants*; VCH: Weinheim, Germany, 1988; Chapter 1, pp 7–19.

(45) Sabatini, A.; Vacca, A.; Gans, P. *Talanta* **1974**, *21*, 53–77.

(46) Sillen, L. G.; Warnqvist, B. *Arkiv. Kemi.* **1968**, *31*, 377–390.

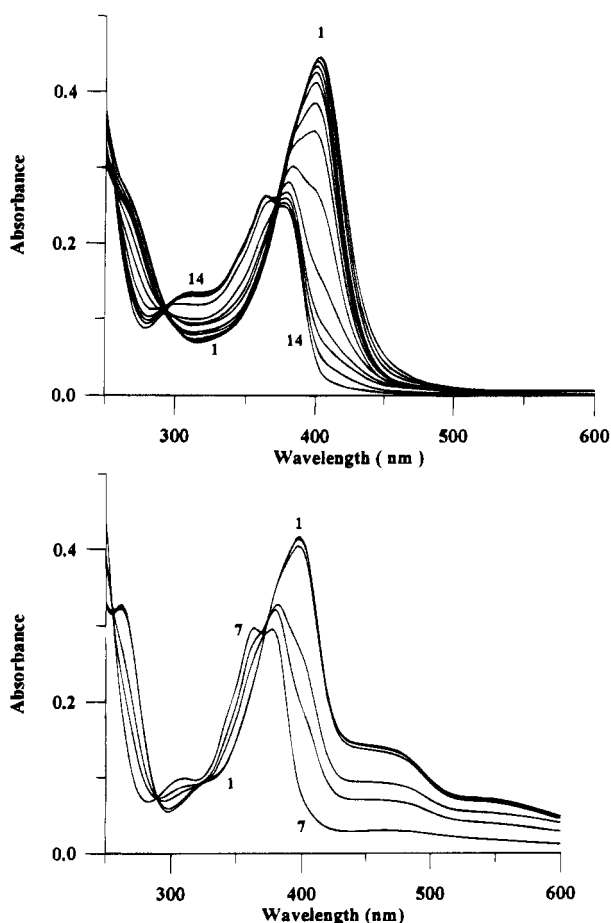


Figure 2. Evolution of the absorption spectra of pyoverdine PaA and its ferric species at different concentrations of protons. Solvent: water. $T = 25.0 \pm 0.1$ °C; $I = 0.1$; $l = 0.2$ cm. (a) $[\text{PaA}]_0 = 7.7 \times 10^{-5}$ M; $[\text{NaOH}] = 0.1$ M. Key: spectrum 1, $\text{p}[\text{H}^+] = 9.8$; spectrum 2, $\text{p}[\text{H}^+] = 9.2$; spectrum 3, $\text{p}[\text{H}^+] = 8.9$; spectrum 4, $\text{p}[\text{H}^+] = 8.4$; spectrum 5, $\text{p}[\text{H}^+] = 7.7$; spectrum 6, $\text{p}[\text{H}^+] = 7.2$; spectrum 7, $\text{p}[\text{H}^+] = 6.8$; spectrum 8, $\text{p}[\text{H}^+] = 6.4$; spectrum 9, $\text{p}[\text{H}^+] = 5.8$; spectrum 10, $\text{p}[\text{H}^+] = 5.7$; spectrum 11, $\text{p}[\text{H}^+] = 4.2$; spectrum 12, $\text{p}[\text{H}^+] = 3.5$; spectrum 13, $\text{p}[\text{H}^+] = 2.7$; spectrum 14, $\text{p}[\text{H}^+] = 1.7$. (b) $[\text{PaAFe(III)}]_0 = 1.30 \times 10^{-4}$ M; $[\text{HCl}] = 1$ M. Key: spectrum 1, $\text{p}[\text{H}^+] = 5.1$; spectrum 2, $\text{p}[\text{H}^+] = 4.0$; spectrum 3, $\text{p}[\text{H}^+] = 3.1$; spectrum 4, $\text{p}[\text{H}^+] = 2.6$; spectrum 5, $\text{p}[\text{H}^+] = 2.1$; spectrum 6, $\text{p}[\text{H}^+] = 1.4$; spectrum 7, $\text{p}[\text{H}^+] = 1.2$.

was 0.1 M NaClO_4 (MERCK, p.a.) and the buffer was a 10^{-2} M sodium carbonate (MERCK, p.a.) and sodium bicarbonate (MERCK, p.a.) mixture. Different proportions of these products⁴⁷ gave a $\text{p}[\text{H}^+]$ between 9 and 11. The hydrogen ion concentration was measured with a Ag/AgCl combined glass electrode (TACUSSEL High Alkalinity, saturated sodium chloride) and a MINISIS 5,000 TACUSSEL millivoltmeter. Electrochemical studies were carried out at a range of potentials varying from -600 to -1000 mV/NHE and scan speeds varying from 5 V s^{-1} to 2.5 mV s^{-1} . An experimental recording is given as an example in Figure 3.

Kinetic Measurements. The formation and dissociation reactions of iron(III) pyoverdine PaA involved both slow and rapid steps. For the rapid steps, a DURRUM GIBSON D-110 stopped-flow spectrophotometer connected to a TEKTRONIX Q-11 fast storage oscilloscope was used. The signal was digitized and stored by a DATALAB DL 905 transient recorder. The corresponding kinetic data were treated on line either with an APPLE II microcomputer and classical software⁴⁸ or with a TANDON computer and the commercial BIOCINE program.⁴⁹ The slow steps were measured with a KONTRON UVIKON 860

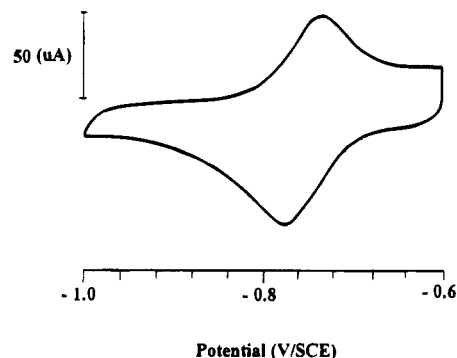


Figure 3. Cyclic voltammogram of the iron(III) pyoverdine PaA complex. Scan speed: 100 mV s^{-1} ; $\text{p}[\text{H}^+] = 9.65$. Solvent: water. $T = 25.0 \pm 0.1$ °C; $I = 0.1$.

spectrophotometer and the kinetic data processed using the BIOCINE software⁴⁹ with an IBM PS2 microcomputer. Rate constant determination and absorbance analysis were performed with the help of the commercial ENZFITTER⁵⁰ program based on a Marquardt algorithm. The solutions were prepared with deionized water. The temperature was maintained at 25.0 ± 0.1 °C and the ionic strength fixed at 2.0 using sodium perchlorate (MERCK, p.a.). The thermodynamic and spectrophotometric data allowed the best experimental conditions for kinetic determinations to be chosen.

Formation kinetics were studied using a stopped-flow technique at 403 nm. Pseudo-first-order conditions with respect to iron(III) were used, pyoverdine PaA concentration being equal to 5×10^{-6} M and iron(III) concentration ($\text{FeCl}_3 \cdot 6\text{H}_2\text{O}$, Merck, p.a.) varying between 5×10^{-5} and 4×10^{-4} M. To avoid the formation and precipitation of a large number of hydroxylated iron(III) forms⁵¹ the experiments were performed in a $\text{p}[\text{H}^+]$ range between 1.8 and 2.3. Using this narrow $\text{p}[\text{H}^+]$ range, the ferric pyoverdine PaA species was obtained with yields superior to 80%. The reaction order with respect to protons was also reduced under these conditions. The activation parameters of the complexation reaction were determined from experiments run at 15.0 ± 0.5 °C; 21.7 ± 0.2 °C; 25.0 ± 0.1 °C; 30.0 ± 0.2 °C and 35.0 ± 0.5 °C.

The acidic dissociation kinetics of ferric pyoverdine PaA species were studied in the presence of excess protons ($0 < \text{p}[\text{H}^+] < 1.5$) and a complete decomplexation ($>90\%$) was obtained. The initial $\text{p}[\text{H}^+]$ of the ferric pyoverdine PaA complex solutions was adjusted to 4.0.

Results

Thermodynamics and Spectrophotometry. The structure of the free siderophore pyoverdine PaA (Figure 1) shows two protonation sites on the lateral chains (arginine and succinic acid) and four involving the iron(III) coordination sites (catechol-type and two hydroxamic acid functions). Taking into account the positive charge of the catechol-type chromophore moiety, the deprotonated free form of pyoverdine PaA was denoted L^{4-} . Six $\text{p}K$ values (Table 1) were determined by acid-base potentiometric titrations of the free siderophore and of its ferric species. The $\text{p}K_3$ and $\text{p}K_4$ values at about 8.1 could not be determined separately by the MINQUAD program⁴⁵ and agree very well with classical values observed for hydroxamic acids.^{52–56} Spectrophotometric titrations of the free siderophore (Figure 2a) have shown the existence of three absorbing species

- (50) Leatherbarrow, J. BIOSOFT, Cambridge, U.K., 1987.
 (51) Sapiezko, R. S.; Patel, R. C.; Matijevic, E. *J. Phys. Chem.* **1977**, *81*, 1061–1068.
 (52) Exner, O.; Simon, W. *Collect. Czech. Chem. Commun.* **1965**, *30*, 4078–4094.
 (53) Brink, C. P.; Crumbliss, A. L. *J. Org. Chem.* **1982**, *47*, 1171–1176.
 (54) Brink, C. P.; Fish, L. L.; Crumbliss, A. L. *J. Org. Chem.* **1985**, *50*, 2277–2281.
 (55) Monzyk, B.; Crumbliss, A. L. *J. Org. Chem.* **1980**, *45*, 4670–4675.
 (56) Ventura, O. N.; Rama, J. B.; Turi, L.; Dannenberg, J. J. *J. Am. Chem. Soc.* **1993**, *115*, 5754–5761.

(47) Perrin, D. D.; Dempsey, B. *Buffer for pH and Metal Ion Control*; Chapman and Hall: New York, 1974; Chapter 9–10, pp 117–173.
 (48) Lagrange, J.; Lagrange, P. *J. Chim. Phys.* **1984**, *81*, 425–431.
 (49) Bio-logic Company, Echirrolles, France, 1991.

Table 1. Protonation Constants of the Free Pyoverdin PaA Ligand and Stability Constants of the Ferric Complexes^a

equilibria	thermodynamic constants $\pm \sigma$	pM $\pm \sigma$
$\text{LH}^{3-} \rightleftharpoons \text{L}^{4-} + \text{H}^+$	$\text{p}K_1 = 12.2 \pm 0.3$	
$\text{LH}_2^{2-} \rightleftharpoons \text{LH}_3^{-} + \text{H}^+$	$\text{p}K_2 = 10.8 \pm 0.3$	
$\text{LH}_3^{-} \rightleftharpoons \text{LH}_2^{2-} + \text{H}^+$	$7.6 \leq \text{p}K_3, \text{p}K_4 \leq 8.6$	
$\text{LH}_4 \rightleftharpoons \text{LH}_3^{-} + \text{H}^+$		27 ± 1
$\text{LH}_5^+ \rightleftharpoons \text{LH}_4 + \text{H}^+$	$\text{p}K_5 = 5.7 \pm 0.2$	
$\text{LH}_6^{2+} \rightleftharpoons \text{LH}_5^+ + \text{H}^+$	$\text{p}K_6 = 4.8 \pm 0.3$	
$\text{L}^{4-} + \text{Fe}^{3+} \rightleftharpoons \text{LFe}^-$	$\log K_{\text{LFe(III)}} = 30.8 \pm 0.3$	
$\text{L}^{4-} + \text{Fe}^{3+} + \text{H}^+ \rightleftharpoons \text{LHFe}$	$\log \beta_{\text{LHFe(III)}} = 43.0 \pm 0.3$	
$\text{L}^{4-} + \text{Fe}^{3+} + 2\text{H}^+ \rightleftharpoons \text{LH}_2\text{Fe}^+$	$\log \beta_{\text{LH}_2\text{Fe(III)}} = 47.8 \pm 0.2$	

^a pM = $-\log [\text{Fe}^{3+}]$ when $[\text{Fe}^{3+}] = 10^{-6}$ M, $[\text{L}] = 10^{-5}$ M and $\text{p}[\text{H}^+] = 7.4$. Solvent: water. $T = 25 \pm 0.1$ °C; $I = 0.1$.

that are $\text{p}[\text{H}^+]$ dependent and correspond to the protonation of the catechol-type chromophore. Due to oxidation of the samples at high $\text{p}[\text{H}^+]$, determination of the absorption spectrum of the deprotonated catechol-type moiety with sufficient accuracy was not possible. The deprotonation constant ($\text{p}K = 5.4 \pm 0.1$) fitted with the LETAGROP program⁴⁶ was compared to the $\text{p}K_5$ value (5.7 ± 0.2) presented in Table 1 and determined by potentiometry. These $\text{p}K$ values were easily attributed to the equilibrium between the diprotonated form of the catechol-type chromophore and its monoprotinated species. The corresponding calculated electronic spectra are presented in Figure 4. With the help of data available in the literature, arginine⁵⁷ ($\text{p}K = 12.48$) and succinic acid⁵⁸ ($\text{p}K = 4.8$) deprotonation constants obtained for pyoverdin PaA under our experimental conditions could be identified respectively as $\text{p}K_1 = 12.2 \pm 0.3$ and $\text{p}K_6 = 4.8 \pm 0.3$. The $\text{p}K_6$ value was confirmed by an acid-base titration of the ferric species for which the peripheral succinic acid is not involved in coordination (Table 1). The $\text{p}K_2$ value is 10.8 ± 0.3 , attributed to the deprotonation of the catechol-type function, was in good agreement, as for the $\text{p}K_5$ value, with data available for hydroxyquinoline protonation properties.^{59,60}

The spectrophotometric titration of the ferric pyoverdin PaA species in water over a large $\text{p}[\text{H}^+]$ range (3.0–9.0) shows a single electronic spectrum with two charge transfer bands at 460 nm and 540 nm (Figure 2b). The spectrophotometric and potentiometric data obtained over a $\text{p}[\text{H}^+]$ range between 4.0 and 1.6, where spectrophotometric variations could be observed (Figure 2b), were processed with the LETAGROP program⁴⁶ and the global thermodynamic constant $\beta_{\text{LH}_2\text{Fe}}$ relative to a diprotonated ferric complex was determined (Table 1). Using results obtained by potentiometric titration of both the free siderophore pyoverdin PaA and its ferric complex for the exterior protonation sites (arginine and succinic acid), the stability constants of the monoprotinated pyoverdin complex LHFe and the deprotonated LFe^- were calculated. These values along with the protonation constants of the free ligand, are listed in Table 1.

The distribution curves obtained with the HALTAFALL program⁶¹ for known and equal concentrations of pyoverdin PaA and iron(III) at various $\text{p}[\text{H}^+]$ values, taking into account the thermodynamic constants presented in Table 1 and the hydrolysis constants⁵¹ related to $\text{Fe}(\text{OH})_2^{2+}$, $\text{Fe}(\text{OH})_2^+$ and $\text{Fe}_2(\text{OH})_2^{4+}$,

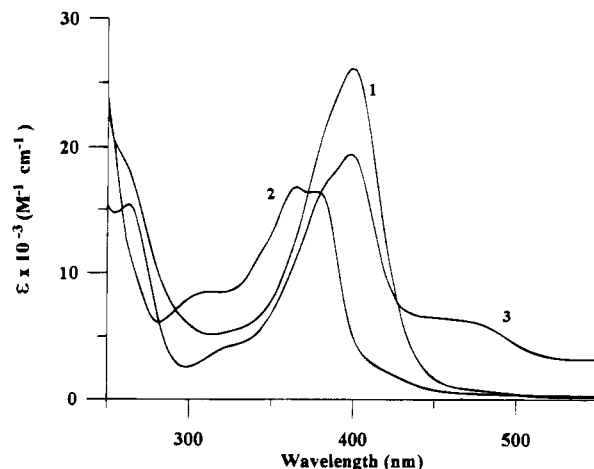


Figure 4. Calculated electronic spectra of the different protonated pyoverdin PaA species and of its ferric complexes. Key: spectrum 1, $\epsilon_{\text{LH}_2^{2-}} = \epsilon_{\text{LH}_3^{-}} = \epsilon_{\text{LH}_4}$; spectrum 2, $\epsilon_{\text{LH}_5^+} = \epsilon_{\text{LH}_6^{2+}}$; spectrum 3, $\epsilon_{\text{LH}_2\text{Fe}^+} = \epsilon_{\text{LHFe}} = \epsilon_{\text{LFe}^-}$. Solvent: water. $T = 25.0$ °C; $I = 0.1$.

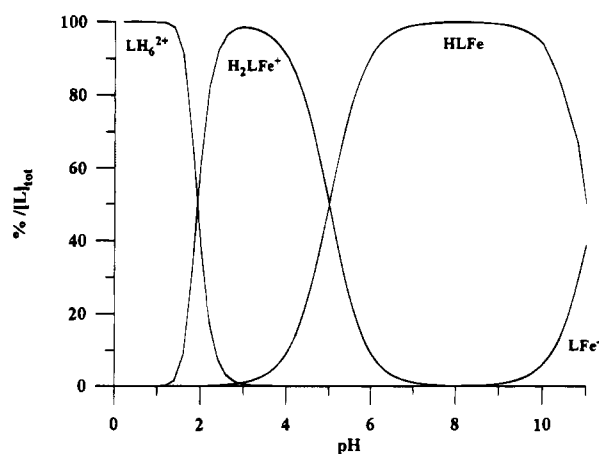


Figure 5. Formation curves of ferric pyoverdin PaA complexes under various acidic conditions. $[\text{PaA}] = [\text{Fe(III)}] = 5 \times 10^{-6}$ M. Solvent: water. $T = 25.0$ °C; $I = 0.1$.

show the formation of the neutral complex LHFe under physiological conditions (Figure 5). At $\text{p}[\text{H}^+]$ values below 1.5, the dissociation of the ferric species is complete.

Electrochemistry. Half reduction potentials were determined for ferric pyoverdin PaA species in a narrow $\text{p}[\text{H}^+]$ range between 9.0 and 10.7. Under these conditions, reversible electrochemical behavior was observed for potential scan speeds below 100 mV s^{-1} and the reduction potential values were independent of $\text{p}[\text{H}^+]$. An average value of the reduction potential has been calculated:

$$E_{1/2} = E_{\text{LHFe}}^{\circ} = -0.51 \pm 0.01 \text{ V/NHE} \quad (1)$$

Using this result, the reduction potential of iron(III) E_{Fe}° (0.77 V/NHE), and the stability constant of the ferric pyoverdin PaA species LHFe (Table 1), the stability constant of the corresponding pyoverdin PaA ferrous complex was calculated according to the following expression:

$$\ln \beta_{\text{LHFe(II)}} = -\frac{(E_{\text{Fe}}^{\circ} - E_{\text{LHFe}}^{\circ})}{0.059} + \ln \beta_{\text{LHFe(III)}} \quad (2)$$

The calculated thermodynamic constants for the pyoverdin PaA ferrous species are $\log K_{\text{LFe(II)}} = 9 \pm 1$, $\log \beta_{\text{LHFe(II)}} = 21 \pm 1$ and $\log \beta_{\text{LH}_2\text{Fe(II)}} = 26 \pm 1$.

Formation Kinetics. At 403 nm a single exponential spectrophotometric increase vs time was recorded which cor-

(57) Albert, A. *Biochem. J.* **1952**, *50*, 690–697.

(58) Yasuda, M.; Yamasaki, K.; Ohtaki, H. *Bull. Chem. Soc. Jpn.* **1960**, *33*, 1067–1070.

(59) Schulman, S.; Fernando, Q. *Tetrahedron* **1968**, *24*, 1777–1783.

(60) Mason, S. F.; Philp, J.; Smith, B. E. *J. Chem. Soc. A* **1968**, 3051–3056.

(61) Ingri, N.; Kakolowics, W.; Sillen, L. G.; Warnqvist, B. *Talanta* **1969**, *14*, 1261–1286.

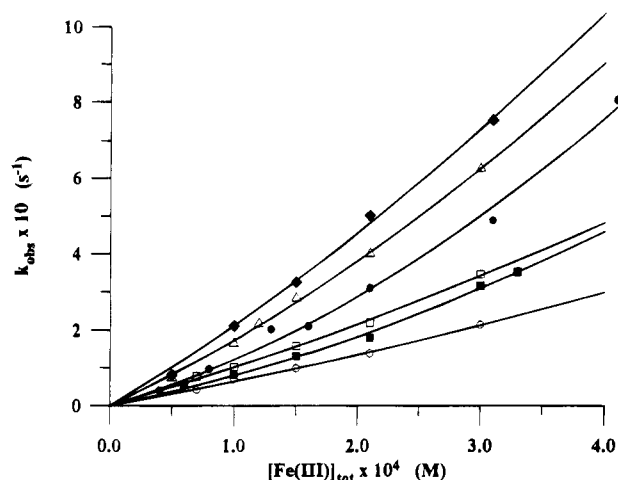


Figure 6. Variation of the experimental rate constant k_{obs} of iron(III) pyoverdine PaA complex formation as a function of $[\text{Fe(III)}]_{\text{tot}}$ and of $[\text{H}^+]$. Key: (\blacklozenge) $[\text{H}^+] = 0.005 \text{ M}$; (\triangle) $[\text{H}^+] = 0.006 \text{ M}$; (\bullet) $[\text{H}^+] = 0.008 \text{ M}$; (\square) $[\text{H}^+] = 0.01 \text{ M}$; (\blacksquare) $[\text{H}^+] = 0.012 \text{ M}$; (\circ) $[\text{H}^+] = 0.015 \text{ M}$. $[\text{PaA}] = 5 \times 10^{-6} \text{ M}$. Solvent: water. $T = 25.0 \pm 0.1 \text{ }^\circ\text{C}$; $l = 2.0$.

responds to the total spectrophotometric signal expected from our studies carried out at equilibrium and also from the dead time of the stopped-flow device (3 ms). The corresponding pseudo-first order constants k_{obs} (s^{-1}) determined at $25.0 \pm 0.1 \text{ }^\circ\text{C}$ at various $\text{p}[\text{H}^+]$ values and concentrations of iron(III) in excess are presented in Figure 6.

The variations of k_{obs} at given $\text{p}[\text{H}^+]$ with the analytical concentrations of iron(III), $[\text{Fe(III)}]_{\text{tot}}$, fitted⁵⁰ the following relationship:

$$k_{\text{obs}} = k_a[\text{Fe(III)}]_{\text{tot}} + k_b[\text{Fe(III)}]_{\text{tot}}^2 \quad (3)$$

with k_{obs} (s^{-1}), k_a ($\text{M}^{-1} \text{s}^{-1}$) and k_b ($\text{M}^{-2} \text{s}^{-1}$). Using a statistical method,⁵⁰ variations of the rate constants k_a and k_b with the analytical concentrations of protons $[\text{H}^+]$ at given concentrations of iron(III) in excess were found to confirm the following mathematical equations with the constants A (s^{-1}), B (s^{-1}), A' ($\text{M}^{-1} \text{s}^{-1}$), A'' (M) and B' (M):

$$k_a = \frac{A + A'[\text{H}^+]}{A'' + [\text{H}^+]} \quad (4)$$

$$k_b = \frac{B}{(B' + [\text{H}^+])^2} \quad (5)$$

The corresponding rate law can be written:

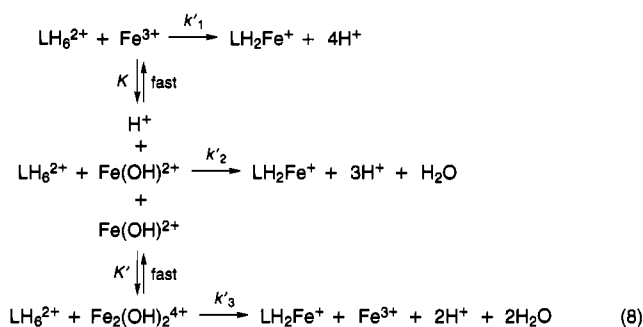
$$v = \left\{ \frac{A + A'[\text{H}^+]}{A'' + [\text{H}^+]} [\text{Fe(III)}]_{\text{tot}} + \frac{B}{(B' + [\text{H}^+])^2} [\text{Fe(III)}]_{\text{tot}}^2 \right\} [\text{LH}_6^{2+}] \quad (6)$$

This result suggests the formation mechanism of a single pyoverdine PaA ferric complex, LH_2Fe^+ , from a single protonated form of free pyoverdine PaA, LH_6^{2+} , via the hydroxylated species of iron(III). The protolytic and dimerization equilibria between the iron(III) species can be considered as fast steps⁶² compared to those involving coordination, and then the corresponding thermodynamic constants⁶³ will be used in the kinetic equations. At equilibrium, under our experimental conditions ($1.8 <$

$\text{p}[\text{H}^+] < 2.3$), the concentrations of the $\text{Fe}(\text{OH})_2^+$ and $\text{Fe}_2(\text{OH})_2^{4+}$ species could be neglected and the total iron(III) concentration written as:

$$\begin{aligned} [\text{Fe(III)}]_{\text{tot}} &= [\text{Fe}^{3+}] + [\text{Fe}(\text{OH})_2^{2+}] \\ &= \left(\frac{K + [\text{H}^+]}{[\text{H}^+]} \right) [\text{Fe}^{3+}] \\ \text{Fe}^{3+} &\rightleftharpoons \text{Fe}(\text{OH})_2^{2+} + \text{H}^+ \end{aligned} \quad (7)$$

For the sake of simplicity, all the water molecules solvating the various iron(III) species have been omitted in our notations. Our kinetic data fit well with a mechanism that takes into account the reactivity of Fe^{3+} , $\text{Fe}(\text{OH})_2^{2+}$ and $\text{Fe}_2(\text{OH})_2^{4+}$:



This mechanism leads to the following rate law:

$$v = \{k'_1[\text{Fe}^{3+}] + k'_2[\text{Fe}(\text{OH})_2^{2+}] + k'_3[\text{Fe}_2(\text{OH})_2^{4+}]\} [\text{LH}_6^{2+}] \quad (9)$$

$$v = \left\{ \frac{k'_2K + k'_1[\text{H}^+]}{K + [\text{H}^+]} [\text{Fe(III)}]_{\text{tot}} + \frac{k'_3K'}{(K + [\text{H}^+])^2} [\text{Fe(III)}]_{\text{tot}}^2 \right\} [\text{LH}_6^{2+}] \quad (10)$$

Comparing eqs 6 and 10, the rate constants at $25 \text{ }^\circ\text{C}$ are calculated as $k'_1 < 80 \text{ M}^{-1} \text{s}^{-1}$, $k'_2 = (7.7 \pm 0.4) 10^3 \text{ M}^{-1} \text{s}^{-1}$ and $k'_3 = (5.0 \pm 0.6) 10^4 \text{ M}^{-1} \text{s}^{-1}$.

The same kinetic measurements were carried out at different temperatures (15 – $35 \text{ }^\circ\text{C}$) and the experimental data obtained at various $\text{p}[\text{H}^+]$ values and iron(III) concentrations for k_a ([4]) are presented in Figure 7. The values of the rate constants k'_1 , k'_2 and k'_3 corresponding respectively to the reactivity of Fe^{3+} , $\text{Fe}(\text{OH})_2^{2+}$ and $\text{Fe}_2(\text{OH})_2^{4+}$ with pyoverdine PaA are collected in Table 2.

Only the kinetic data collected for the reactivity of the $\text{Fe}(\text{OH})_2^{2+}$ species were accurate enough under our experimental conditions to allow the determination of the activation parameters $\Delta H^\ddagger = 11.3 \pm 0.6 \text{ kcal M}^{-1}$ and $\Delta S^\ddagger = -3 \pm 3 \text{ cal M}^{-1} \text{K}^{-1}$ by an Eyring plot.

Dissociation Kinetics. At $\text{p}[\text{H}^+] 1.5$ the complete dissociation kinetics of the diprotonated ferric pyoverdine PaA complex were studied in water. The reactant LH_2Fe^+ was prepared at $\text{p}[\text{H}^+] 4.0$. According to the distribution curves previously presented (Figure 5), the global reaction can be written as:



(62) Birus, M.; Kujundzic, N.; Pribanic, M. *Prog. Reaction Kinet.* **1993**, *18*, 171–271.

(63) Milburn, R. M.; Vosburgh, W. C. *J. Am. Chem. Soc.* **1955**, *77*, 1352–1355.

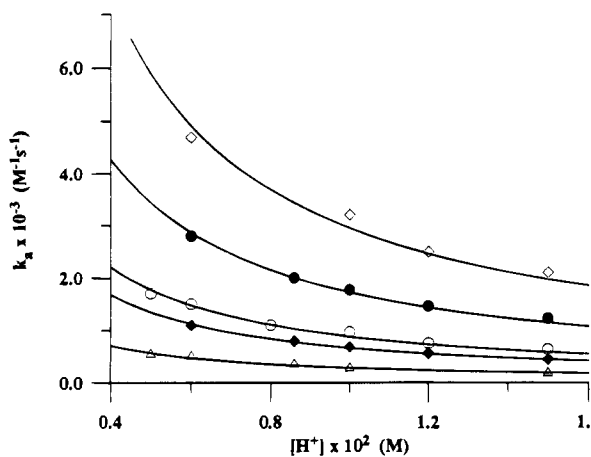


Figure 7. Ferric pyoverdine PaA formation: Variation of apparent rate constant k_a with $[H^+]$ and temperatures. Key: (Δ) $T = 15.0$ °C; (\circ) $T = 21.7$ °C; (\square) $T = 25.0$ °C; (\bullet) $T = 30.1$ °C; (\diamond) $T = 35.0$ °C. Solvent: water. $I = 2.0$.

Table 2. Variation of the Second-Order Iron(III) Pyoverdine PaA Complex Formation Rate Constants Related to Fe^{3+} , $Fe(OH)^{2+}$, and $Fe_2(OH)_2^{4+}$ with Temperature^a

T (°C)	kinetic parameters		
	$(k'_1 \pm 2\sigma)$ ($M^{-1} s^{-1}$)	$(k'_2 \pm 2\sigma) \times 10^{-3}$ ($M^{-1} s^{-1}$)	$(k'_3 \pm 2\sigma) \times 10^{-4}$ ($M^{-1} s^{-1}$)
15.0 ± 0.5	<40	4.0 ± 0.6	
21.7 ± 0.2	<60	6.2 ± 0.4	
25.0 ± 0.1	<80	7.7 ± 0.4	5.0 ± 0.6
30.1 ± 0.2	<100	11.0 ± 0.6	
35.0 ± 0.5	<400	15 ± 1	

^a Solvent: water. $I = 2.0$.

The free iron(III) species liberated by the reaction are in fast equilibrium,⁶² the major final species being Fe^{3+} and $FeOH^{2+}$ in our strongly acidic conditions.

Three exponential spectrophotometric signals have been recorded vs time at 403 nm under pseudo-first order conditions with respect to the protons (Figure 8). Using the stopped-flow method, a large loss of amplitude (50% of the spectrophotometric amplitude at equilibrium) has been observed during the dead time (3 ms) of our device and two exponential decays have been measured, in the respective time ranges of milliseconds and minutes. A final slower exponential decay was detected by classical absorption spectrophotometry. For increased simplicity, the different steps were successively denoted 1, 2, 3, and 4, as indicated in Figure 8.

The values of the pseudo-first order rate constants $k_{obs,2}$, $k_{obs,3}$, and $k_{obs,4}$ related to steps 2–4 respectively were determined and collected in Table 3.

The variations of $k_{obs,2}$ and $k_{obs,3}$ were found to be linear with the analytical $[H^+]$ concentrations in the entire $p[H^+]$ range investigated and the ordinates at the origin could be determined with good accuracy. Variations of $k_{obs,4}$ with $[H^+]$ were linear at high $p[H^+]$ values. At lower $p[H^+]$ values, in agreement with results obtained for ferrioxamine B by Birus et al.,⁶⁴ we were obliged to take into account a more sophisticated mathematical approach which provided kinetic results consistent with those previously obtained for the formation mechanism. These experimental data suggest the formation of three intermediate protonated ferric pyoverdine PaA complexes I_1 , I_2 , and I_3 leading to the release of the metal. The ordinates at the origin could be attributed to the back reaction of the equilibria K_{I_2} and K_{I_3} .

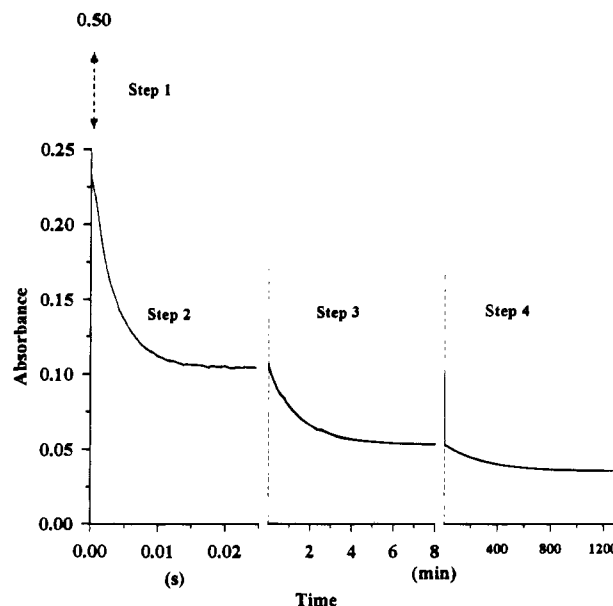


Figure 8. Dissociation kinetics of the ferric pyoverdine PaA species. $[PaAFe(III)]_0 = 3.1 \times 10^{-5}$ M; $[H^+] = 0.15$ M. Solvent: water. $T = 25.0 \pm 0.1$ °C; $I = 2.0$; $l = 1$ cm; $\lambda = 403$ nm.

Table 3. Variation of the Pseudo-First-Order Constants for the Acidic Dissociation of Ferric Pyoverdine PaA with Proton Concentration^a

$[H^+]$ (M)	$(k_{obs,2} \pm 2\sigma) \times 10^{-2}$ (s^{-1})	$(k_{obs,3} \pm 2\sigma) \times 10^2$ (s^{-1})	$(k_{obs,4} \pm 2\sigma) \times 10^4$ (s^{-1})
0.025	0.53 ± 0.01		
0.035	0.78 ± 0.03		
0.045	1.07 ± 0.03		0.45 ± 0.01
0.051	1.28 ± 0.03	0.78 ± 0.02	0.50 ± 0.01
0.065	1.36 ± 0.05		0.61 ± 0.01
0.077	1.80 ± 0.06	0.60 ± 0.02	0.30 ± 0.02
0.101	2.20 ± 0.06	0.87 ± 0.02	
0.103	2.19 ± 0.07	0.80 ± 0.02	
0.125	2.65 ± 0.07	1.17 ± 0.03	
0.128		1.00 ± 0.02	0.39 ± 0.07
0.152	3.4 ± 0.1	1.04 ± 0.05	
0.154		1.20 ± 0.03	0.50 ± 0.01
0.192		1.37 ± 0.03	
0.203		1.46 ± 0.04	0.60 ± 0.02
0.256			0.81 ± 0.02
0.304		2.50 ± 0.06	
0.375		3.34 ± 0.05	1.5 ± 0.2
0.384		2.72 ± 0.05	
0.504		4.9 ± 0.1	
0.605		6.1 ± 0.1	1.9 ± 0.3
0.703		6.2 ± 0.2	2.4 ± 0.2
0.705		6.6 ± 0.2	2.33 ± 0.04
0.769		7.31 ± 0.05	2.8 ± 0.2
0.806		8.3 ± 0.2	
0.907		9.1 ± 0.2	
1.014		10.0 ± 0.2	

^a $[Pyoverdine\ PaAFe(III)] = 3.1 \times 10^{-5}$ M. Solvent: water. $T = 25.0 \pm 0.1$ °C; $I = 2.0$.

For the final step, a proton independent dissociation pathway via $Fe(OH)^{2+}$ was envisioned.^{65–67} By analogy with steps 2 and 3, an initial bimolecular attack of the protons was proposed for step 1. This hypothesis will be checked, however, by analysis of the spectrophotometric amplitudes. The corresponding mechanism is proposed in Scheme 1. Taking into consideration the second elementary step written in Scheme 1 and the

(64) Birus, M.; Bradic, Z.; Krznaric, G.; Kujundzic, N.; Pribanic, M.; Wilkins, P. C.; Wilkins, R. G. *Inorg. Chem.* **1987**, *26*, 1000–1005.

(65) Birus, M.; Bradic, Z.; Kujundzic, N.; Pribanic, M.; Wilkins, P. C.; Wilkins, R. G. *Inorg. Chem.* **1985**, *24*, 3980–3983.

(66) Monzyk, B.; Crumbliss, A. L. *J. Am. Chem. Soc.* **1979**, *101*, 6203–6213.

experimental data presented in Table 3, the values of the rate constants k_2 and k_{-2} were determined (Table 4) according to the relationship:

$$k_{\text{obs},2} = k_{-2} + k_2[\text{H}^+] \quad (12)$$

By analyzing the spectrophotometric amplitude measured at the end of the two first steps $A_{\infty,2}$ vs $p[\text{H}^+]$ and taking into account the equilibria K_{I_1} and K_{I_2} (Scheme 1), the expression of $A_{\infty,2}$ (Figure 9) vs the concentrations of protons can be processed using a nonlinear least squares method:

$$\frac{A_{\infty,2}}{[\text{LH}_2\text{Fe}^+]_{\text{tot}}} = \frac{\epsilon_{\text{LH}_2\text{Fe}^+} + \epsilon_{I_1}K_{I_1}[\text{H}^+] + \epsilon_{I_2}K_{I_1}K_{I_2}[\text{H}^+]^2}{1 + K_{I_1}[\text{H}^+] + K_{I_1}K_{I_2}[\text{H}^+]^2} \quad (13)$$

The absorption coefficients of intermediates I_1 and I_2 at 403 nm and the stability constants K_{I_1} and K_{I_2} were calculated and are presented in Table 4.

According to the kinetic data presented in Table 3, the rate constants k_3 and k_{-3} were obtained by eq 14 and their values are presented in Table 4. The expression of the spectrophotometric absorbance $A_{\infty,3}$ measured at 403 nm (Figure 9) and at the end of the third elementary step (Scheme 1) could be processed vs the concentrations of protons:

$$k_{\text{obs},3} = k_{-3} + k_3[\text{H}^+] \quad (14)$$

metric absorbance $A_{\infty,3}$ measured at 403 nm (Figure 9) and at the end of the third elementary step (Scheme 1) could be processed vs the concentrations of protons:

$$\frac{A_{\infty,3}}{[\text{LH}_2\text{Fe}^+]_{\text{tot}}} = \frac{\epsilon_{\text{LH}_2\text{Fe}^+} + \epsilon_{I_1}K_{I_1}[\text{H}^+] + \epsilon_{I_2}K_{I_1}K_{I_2}[\text{H}^+]^2 + \epsilon_{I_3}K_{I_1}K_{I_2}K_{I_3}[\text{H}^+]^3}{1 + K_{I_1}[\text{H}^+] + K_{I_1}K_{I_2}[\text{H}^+]^2 + K_{I_1}K_{I_2}K_{I_3}[\text{H}^+]^3} \quad (15)$$

The values of the absorption coefficient ϵ_{I_3} at 403 nm of the intermediate complex I_3 and of the stability constant K_{I_3} were obtained (Table 4) by a nonlinear least squares method⁵⁰ and the values previously determined by the relationship in (13). If the mechanism proposed in Scheme 1 is considered, the variations of the rate constants $k_{\text{obs},4}$ vs $[\text{H}^+]$ for the fourth and slowest step will confirm the following equation:

$$k_{\text{obs},4} = \frac{(k_5 + k_4[\text{H}^+])K_{I_3}[\text{H}^+]}{1 + K_{I_3}[\text{H}^+]} + \left(k_{-4} + \frac{k_{-5}K}{K + [\text{H}^+]} \right) ([\text{Fe(III)}]_e + [\text{LH}_6^{2+}]_e) \quad (16)$$

$[\text{LH}_6^{2+}]_e$ and $[\text{Fe(III)}]_e$ are the total equilibrium concentrations of ligand and metal under our experimental conditions.

Using a nonlinear least squares method,⁵⁰ data previously presented in this paper, the K value available in the literature⁶³ and the K_{I_3} determined for the preceding step, the rate constants k_4 and k_{-4} (Table 4) related to the proton assisted final dissociation step and k_5 and k_{-5} (Table 4) related to the proton independent step were determined.

The variations of the final spectrophotometric absorbance for the fourth step vs proton concentrations (Figure 9) allowed us, using a nonlinear least squares program,⁵⁰ to determine the stability constant K_{Fe} (Scheme 1) and the extinction coefficient of the free ligand according to the following relationship:

$$\frac{A_{\infty,4}}{C_{\text{tot}}} = \left\{ \epsilon_{\text{LH}_2\text{Fe}^+} + \epsilon_{I_1}K_{I_1}[\text{H}^+] + \epsilon_{I_2}K_{I_1}K_{I_2}[\text{H}^+]^2 + \epsilon_{I_3}K_{I_1}K_{I_2}K_{I_3}[\text{H}^+]^3 + \epsilon_{\text{LH}_6^{2+}}K_{I_1}K_{I_2}K_{I_3}K_{\text{Fe}} \frac{[\text{H}^+]^4}{[\text{Fe}]_e} \right\} \left\{ 1 + K_{I_1}[\text{H}^+] + K_{I_1}K_{I_2}[\text{H}^+]^2 + K_{I_1}K_{I_2}K_{I_3}[\text{H}^+]^3 + K_{I_1}K_{I_2}K_{I_3}K_{\text{Fe}} \frac{[\text{H}^+]^4}{[\text{Fe}]_e} \right\} \quad (17)$$

$[\text{LH}_6^{2+}]_e$ and $[\text{Fe(III)}]_e$ are the total equilibrium concentrations of ligand and metal under our experimental conditions.

The values of K_{I_1} , K_{I_2} , and K_{I_3} related to the preceding steps were used as well as the value of the thermodynamic stability constant of the ferric pyoverdin PaA complex (Table 4) which was necessary for calculations of the equilibrium iron(III) concentrations. Calculated values of both the extinction coefficient at 403 nm of the free pyoverdin PaA, LH_6^{2+} , and the thermodynamic constant $K_{\text{Fe}} = k_4/k_{-4}$ were in good agreement with the previously determined spectrophotometric and kinetic data.

Discussion

Equilibrium Studies. The pK_2 value related to the first protonation constant of the hydroxyquinoline type moiety of pyoverdin PaA (Table 1) is respectively two or three orders of magnitude larger than the pK_a values of 7-hydroxyquinoline or 6-hydroxyquinoline^{59, 60} (Table 5). Comparison between the phenol pK_a value⁶⁸ and the catechol $pK_{a,1}$ value^{69,70} shows an identical stabilization effect due to hydrogen bonds between the two adjacent hydroxyl groups of catechol (Table 5). The decrease of about two orders of magnitude of the first protonation constant of pyoverdin PaA hydroxyquinoline-type function compared to the corresponding protonation constant of catechol is similar to the decrease observed for 7-hydroxyquinoline and 6-hydroxyquinoline^{59,60} compared to phenol⁶⁸ (Table 5). The electronegativity of the oxygen atom of hydroxyquinoline is lower than that of phenol, this effect being due to greater electron delocalization.

The second protonation constant of the fluorescent chromophore of pyoverdin PaA is about three orders of magnitude lower than the corresponding second protonation of catechol^{69,70} (Table 5). The second protonation constant of catechol is similar to the protonation constant of phenol, the second protonation constant of the hydroxyquinoline-type group of pyoverdin PaA being more than one order of magnitude lower than the protonation constant of 6-hydroxyquinoline^{59,60} (Table 5). This effect could be attributed to the proximity of the second proton in position 6 and the positive charge borne by the chromophore of pyoverdin PaA (Figure 1) and would explain the large $\Delta pK = pK_5 - pK_2 = 5.1$ observed.

The two protonation constants related to the two hydroxamate groups of pyoverdin PaA could not be accurately distinguished under our experimental conditions (Table 1). Nevertheless, taking into account the statistical effect between the two thermodynamic constants, our results are in good agreement with the data obtained by Brink et al.^{53,54} for hydroxamic acids bearing an alkyl substituent on the nitrogen atom. These authors

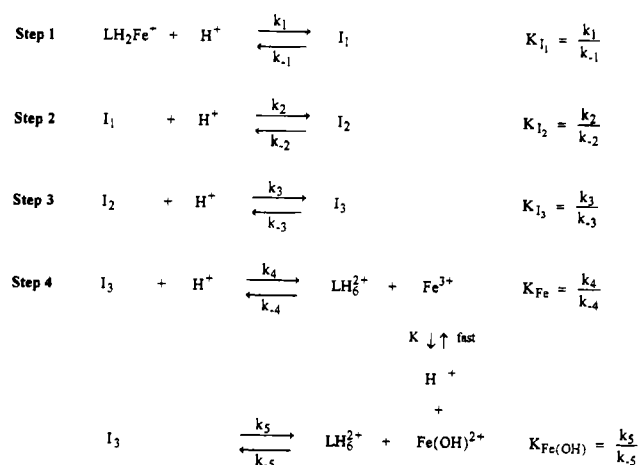
(68) Bordwell, F. G.; Cooper, G. D. *J. Am. Chem. Soc.* **1952**, *74*, 1058–1060.

(69) Tyson, C. A.; Martell, A. E. *J. Am. Chem. Soc.* **1968**, *90*, 3379–3386.

(70) Avdeef, A. A.; Sofen, S. R.; Bregante, T. L.; Raymond, K. N. *J. Am. Chem. Soc.* **1978**, *100*, 5362–5369.

(67) Monzyk, B.; Crumbliss, A. L. *J. Am. Chem. Soc.* **1982**, *104*, 4921–4929.

Scheme 1



have shown that a *N*-methyl substituent decreases the *pK* value of the hydroxamic acid (Table 6), the role of substituents on the carbonyl function being less significant. In pyoverdin PaA, the two hydroxamic acids are identically linked to the peptidic chain by a propyl chain on the nitrogen atom and similar decreases in *pK*₃ and *pK*₄ were observed (Table 1). For comparison, *pK*_a values available for trihydroxamate siderophores are listed in Table 6. The *pK*₃ and *pK*₄ values determined for the hydroxamate groups of pyoverdin PaA are in good agreement with the order of magnitude of the protonation constant of the third hydroxamate of trihydroxamate compounds.^{71–73} This comparison reflects substituent and statistical effects on the *pK*₃ and *pK*₄ values of pyoverdin PaA.

The *pK*₁ and *pK*₆ values (Table 1), respectively attributed to the exterior protonation sites of pyoverdin PaA, are in agreement with the *pK* values available in the literature for arginine⁵⁷ and succinic acid.⁵⁸

Using the stability constant ($\log \beta_{\text{LH}_2\text{Fe}^{2+}} = 47.8 \pm 0.2$) determined in acidic conditions for the pyoverdin PaA complex with protonated arginine and succinate exterior sites the stability constant of the neutral monoprotonated complex LHFe ($\log \beta_{\text{LHFe}} = 43.0 \pm 0.3$) was calculated. This LHFe stability constant corresponds to the protonation of succinic acid and is the only ferric species formed at physiological pH (Figure 5).

In order to compare the iron(III) complexation properties of pyoverdin PaA with other natural siderophores, the corresponding *pM* values, which measure the equilibrium concentration of iron(III) at physiological $\text{p[H}^+]$ (7.4) and under given ligand and metal concentrations, are listed in Table 7. In spite of the presence of the catechol-type moiety in pyoverdin PaA, the *pM* value obtained for this siderophore is similar to those of linear trihydroxamates (coprogen,⁷¹ ferrioxamine B⁷²). Enterobactin⁷⁴ with three catecholate coordination sites shows a *pM* value which is about eight orders of magnitude larger than that of pyoverdin PaA (Table 7). This result reflects the decrease in *pK* values observed for the dihydroxyquinoline-type group of pyoverdin PaA compared to catechol^{69,70} (Table 5). An enhancement of about three orders of magnitude of the *pM* value is induced by the replacement of hydroxycarboxylic acid in aerobactin¹³ by a catecholate-type function in pyoverdin PaA,

the other coordination sites being for these two siderophores two hydroxamates.

Protonation of the catechol-type chromophore of free pyoverdin PaA induces a blue shift of the absorption spectra and a decrease in extinction coefficients (Figure 4). These observations are in agreement with data available for 6- and 7-hydroxyquinoline.^{59,60} The electronic spectrum calculated for the pyoverdin PaA ferric species shows two ligand to ferric ion charge transfer bands respectively centered at 460 nm ($\epsilon_{460} = 6500 \text{ M}^{-1} \text{ cm}^{-1}$) for the two hydroxamate coordination sites and at 540 nm ($\epsilon_{540} = 3500 \text{ M}^{-1} \text{ cm}^{-1}$) for the catecholate-type site. Shifts to longer wavelengths and enhancement of the absorption properties were observed when compared to the trihydroxamate complex ferrioxamine B⁶⁷ ($\lambda_{\text{max}} = 425 \text{ nm}$, $\epsilon_{425} = 2600 \text{ M}^{-1} \text{ cm}^{-1}$) and the triccatecholate complex, ferrienterobactin⁷⁴ ($\lambda_{\text{max}} = 495 \text{ nm}$, $\epsilon_{495} = 5600 \text{ M}^{-1} \text{ cm}^{-1}$).

The reduction potential of the ferric pyoverdin PaA complex was measured by cyclic voltammetry. The potential is more than 200 mV less negative than that of the enterobactin triccatecholate siderophore, enterobactin⁷⁴ and slightly more negative than that of the trihydroxamate siderophores (ferrioxamine B,⁷⁵ coprogen⁷¹) as shown in Table 8. Within experimental error, the stability constant of the ferrous pyoverdin PaA complex is very similar to that calculated for ferrioxamine B⁷⁵ or coprogen⁷¹ (Table 8).

Compared to enterobactin, a destabilization of the ferrous complexes of more than ten orders of magnitude is observed for ferrioxamine B and pyoverdin PaA. A decrease of five orders of magnitude has been measured by Harris et al.¹³ for aerobactin when the catecholate-type coordination site of pyoverdin PaA is replaced by a hydroxycarboxylic acid. In conclusion, the fluorescent pyoverdin PaA chromophore showed very similar ligation properties of iron(III) and iron(II) as hydroxamate coordination sites. This similarity leads us to propose the same biological release of iron(III) for pyoverdin PaA and trihydroxamate siderophores via a possible reduction step of the ferric complexes by common physiological reductants.

Kinetic Studies. The formation reaction of the iron(III) pyoverdin PaA complex in acidic conditions ($1.8 \text{ p[H}^+]$ 2.3) showed a single initial rate limiting step. The proposed mechanism involves three iron(III) species in fast equilibrium,⁶² Fe^{3+} , Fe(OH)_2^{2+} and $\text{Fe}_2(\text{OH})_2^{4+}$. No reactivity of the dihydroxylated species Fe(OH)_2^+ was observed (Table 2). Only the fully protonated form of the free siderophore, LH_6^{2+} , which is the only ligand species present at equilibrium (Figure 5) takes part in this mechanism. Other protonated forms of free pyoverdin PaA have been taken into account, such as LH_5^+ , but did not provide results consistent with data available in the literature (Table 9). No protonic ambiguity⁶² has been observed in this mechanism.

Due to the lack of reactivity between pyoverdin PaA and the major thermodynamic ferric species, Fe^{3+} , present under our experimental conditions, (Figure 8) data more accurate than the superior limit of the bimolecular rate constant k'_1 could not be provided (Table 9). The order of magnitude of this result is in good agreement with of the corresponding rate constant k'_1 determined with hydroxamic acids^{66,76,77} at 25 °C (Table 9).

More precise results have been obtained for the formation pathway of the ferric pyoverdin PaA complex via the mono-

(71) Wong, G. B.; Kappel, M. J.; Raymond, K. N.; Matzanke, B.; Winkelmann, G. *J. Am. Chem. Soc.* **1983**, *105*, 810–815.

(72) Schwarzenbach, G.; Schwarzenbach, K. *Helv. Chim. Acta* **1963**, *154*, 1391–1400.

(73) Anderegg, G.; L'Eplattenier, F.; Schwarzenbach, G. *Helv. Chim. Acta* **1963**, *46*, 1409–1422.

(74) Lee, C. W.; Ecker, D. J.; Raymond, K. N. *J. Am. Chem. Soc.* **1985**, *107*, 6920–6923.

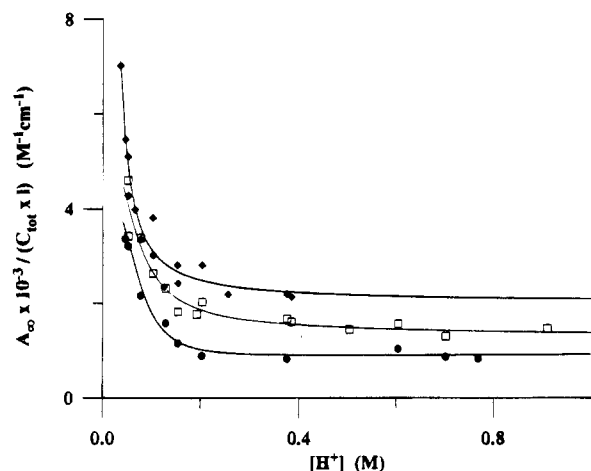
(75) Wawrousek, E. F.; McArdle, J. V. *J. Inorg. Biochem.* **1982**, *17*, 169–183.

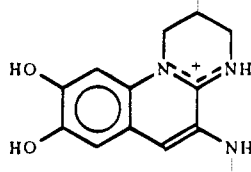
(76) Brink, C. P.; Crumbliss, A. L. *Inorg. Chem.* **1984**, *23*, 4708–4718.

(77) Funahashi, S.; Ishihara, K.; Tanaka, M. *Inorg. Chem.* **1983**, *22*, 2070–2073.

Table 4. Kinetic, Thermodynamic, and Spectrophotometric Parameters Determined for the Acidic Dissociation of the Iron(III) Pyoverdin PaA Complexes^a

elementary steps	rate consts	thermodynamic consts	spectrophotometric data, ϵ ($M^{-1} \text{ cm}^{-1}$) at $\lambda = 403 \text{ nm}$
step 1		$K_{11} < 1000 \text{ M}^{-1}$	$\epsilon_{\text{LH}_2\text{Fe}^+} = 19500 \pm 100$ $\epsilon_{11} = 10000 \pm 2000$
step 2	$k_2 = 1800 \pm 200 \text{ M}^{-1} \text{ s}^{-1}$ $k_{-2} = 20 \pm 10 \text{ s}^{-1}$	$K_{12} = 100 \pm 20 \text{ M}^{-1}$ $k_2/k_{-2} = 90 \pm 60 \text{ M}^{-1}$	$\epsilon_{12} = 2100 \pm 200$
step 3	$k_3 = (7.5 \pm 0.5) \times 10^{-2} \text{ M}^{-1} \text{ s}^{-1}$ $k_{-3} = (4 \pm 2) \times 10^{-3} \text{ s}^{-1}$	$K_{13} = 8 \pm 4 \text{ M}^{-1}$ $k_3/k_{-3} = 20 \pm 10 \text{ M}^{-1}$	$\epsilon_{13} = 1400 \pm 200$
step 4	$k_4 = (3.2 \pm 0.6) \times 10^{-4} \text{ M}^{-1} \text{ s}^{-1}$ $k_{-4} = 6 \pm 2 \text{ M}^{-1} \text{ s}^{-1}$ $k_5 > 6 \times 10^{-5} \text{ s}^{-1}$ $k_{-5} \approx 10^3 \text{ M}^{-1} \text{ s}^{-1}$	$K_{\text{Fe}} = (1.4 \pm 0.6) \times 10^{-4}$ $k_4/k_{-4} = (5 \pm 3) \times 10^{-5}$	$\epsilon_{\text{LH}_6^{2+}} = 800 \pm 100$ $\epsilon_{\text{Fe(III)}} = 0$

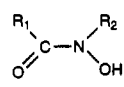
^a Solvent: water. $T = 25.0 \pm 0.1 \text{ }^\circ\text{C}$; $I = 2.0$.**Figure 9.** Variation of the absorbance at the end of each step of the dissociation of the ferric pyoverdin PaA complex. Key: (\blacklozenge) $A_{\infty,2}$; (\square) $A_{\infty,3}$; (\bullet) $A_{\infty,4}$. Solvent: water. $T = 25.0 \pm 0.1 \text{ }^\circ\text{C}$; $I = 2.0$; $l = 1 \text{ cm}$; $\lambda = 403 \text{ nm}$.**Table 5.** Comparison of the Protonation for the Constants 2,3-Diamino-6,7-hydroxyquinoline Moiety of Pyoverdin PaA with Those of Model Compounds^a

protonation sites	pK_a
phenol ⁶⁸	$pK_a = 9.98$
catechol ⁶⁹	$pK_{a,1} = 12.8$ $pK_{a,2} = 9.45$
catechol ⁷⁰	$pK_{a,1} = 13.00$ $pK_{a,2} = 9.23$
6-hydroxyquinoline ^{59,60}	$pK_a = 7.02$
7-hydroxyquinoline ^{59,60}	$pK_a = 8.32$
	$pK_{a,1} = 10.8$ $pK_{a,2} = 5.7$
pyoverdin PaA	

^a Solvent: water. $T = 25.0 \pm 0.1 \text{ }^\circ\text{C}$; $I = 0.1$.

hydroxylated iron(III) species, $\text{Fe}(\text{OH})^{2+}$. Within experimental error, the second order rate constant $k'_2 = 7.7 \times 10^3 \text{ M}^{-1} \text{ s}^{-1}$ at $25 \text{ }^\circ\text{C}$ is identical to the corresponding kinetic value determined for acetohydroxamic acid⁷⁷ (Table 9). Considering either various hydroxamates and catecholates or a natural trihydroxamate siderophore, no significant variation of the rate constant k'_2 was observed with the nature and the structure of the different ligands (Table 9). These data suggest a classical dissociative Eigen–Wilkins mechanism⁷⁸ with a fast formation step of

Table 6. pK_a Values of Various Hydroxamic Compounds^a

	pK_a		
Hydroxamic Acids ^{53,54}			
	$R_1 = \text{CH}_3$; $R_2 = \text{H}$	9.02	
	$R_1 = \text{CH}_3$; $R_2 = \text{CH}_3$	8.65	
Dihydroxamate Compounds			
rhodotorulic acid ⁹²	9.44	8.49	
Trihydroxamate Compounds			
ferrichrome ⁷³	9.83	9.00	8.11
ferrichrysin ⁷³	10.01	9.02	8.17
ferrioxamine B ⁷²	9.70	9.03	8.39
ferrioxamine E ⁷²	9.89	9.42	8.65
coprogen ⁷¹	9.16	8.86	7.63

^a Solvent: water. $T = 25.0 \pm 0.1 \text{ }^\circ\text{C}$; $I = 0.1$.**Table 7.** pM Values² for Pyoverdin PaA and Various Natural Siderophores^a

	pM
Triccatecholate Siderophores	
enterobactin ⁷⁴	35.5
Trihydroxamate Siderophores	
ferrichrome ⁷²	25.2
ferrioxamine B ⁷²	26.6
ferrioxamine E ⁷²	27.7
coprogen ⁷¹	27.5
Dihydroxamate Siderophores	
rhodotorulic acid ⁹²	21.76
Mixed Siderophores	
two hydroxamates and one hydroxyacid	
aerobactin ¹³	23.3
two hydroxamates and one catecholate-type	
pyoverdin PaA	27

^a $pM = -\log [\text{Fe}^{3+}]$ when $[\text{Fe}^{3+}] = 10^{-6} \text{ M}$, $[\text{L}] = 10^{-5} \text{ M}$, and $p[\text{H}^+] = 7.4$.

an outer-sphere complex (K_{os}) followed by a rate limiting step which involves the desolvation of the metal (k_{ex}):

$$k_{\text{Fe}(\text{OH})} = K_{\text{os}} k_{\text{ex}} \quad (18)$$

Since it was difficult to consider pyoverdin PaA as a spherical cation and to evaluate the closest approach distance between LH_6^{2+} and $\text{Fe}(\text{OH})^{2+}$, the K_{os} value⁷⁹ determined for desferri-ferrioxamine B was used instead of calculating it by the Eigen–Fuoss relationship.⁸⁰ Similarities in the peptidic nature, chemi-

(78) Eigen, M.; Wilkins, R. G. *Mechanism of Inorganic Reactions*. *Adv. Chem. Ser.* **1965**, 55–67.(79) Batinic-Haberle, I.; Birus, M.; Pribanic, M. *Inorg. Chem.* **1991**, 30, 4882–4887.(80) Fuoss, R. M. *J. Am. Chem. Soc.* **1958**, 80, 5059–5061.

Table 8. Iron(III) and Iron(II) Thermodynamic Constants and Reduction Potentials of Pyoverdine PaA Complexes and Various Natural Siderophores

coordination sites	siderophores	reduction potentials (mV/NHE)	log $K_{LFe(III)}$	log $K_{LFe(II)}$
three hydroxamates	ferrichrome A ⁷⁵	-448	32.0	11.3
	ferrioxamine B ⁷⁵	-468	30.5	9.5
	coprogen ⁷¹	-447	30.2	9.6
three catecholates	enterobactin ⁷⁴	-750	52	22.2
two hydroxamates and one hydroxyacid	aerobactin ¹³	-336	22.5	3.8
two hydroxamates and one catecholate-type	pyoverdine PaA	-510	30.8	9.0

Table 9. Reactivity of Fe^{3+} (k_1), $Fe(OH)^{2+}$ (k_2), and $Fe_2(OH)_2^{4+}$ (k_3) with Pyoverdine PaA and Various Hydroxamate and Catecholate Compounds

compounds	k_1 ($M^{-1} s^{-1}$)	k_2 ($M^{-1} s^{-1}$)	k_3 ($M^{-1} s^{-1}$)
pyoverdine PaA	<80	7.7×10^3	5.0×10^4
acetohydroxamic acid ⁷⁷		5.7×10^3	8.1×10^3
substituted hydroxamic acids ^{66,76}	1.2–4.4	$(0.67–4.3) \times 10^3$	
catechol ⁸⁵		3.1×10^3	
substituted catecholate ⁸⁷		$(1.7–3.3) \times 10^3$	$(4.5–220) \times 10^5$
desferriferrioxamine B ⁶²		3.6×10^3	

cal structure and size between pyoverdine PaA and desferriferrioxamine B support this choice, although the positive charge of the two siderophores is different, pyoverdine PaA bearing two positive charges on its LH_6^{2+} species and desferriferrioxamine B a single charge on its fully protonated form. Using $k_{Fe(OH)}$ determined for pyoverdine PaA and K_{os} determined for desferriferrioxamine B⁷⁹ ($K_{os} = 3 \times 10^{-2} M^{-1}$), $k_{ex} = 2 \times 10^5 s^{-1}$ related to the water exchange process of $Fe(OH)^{2+}$ was calculated. This result is in excellent agreement with the rate constant value ($k_{ex} = 1.4 \times 10^5 s^{-1}$) obtained for $Fe(OH)^{2+}$ from NMR measurements.⁸¹

Activation parameters calculated for the reaction of the $Fe(OH)^{2+}$ species with pyoverdine PaA ($\Delta H^\ddagger = 11.3 \text{ kcal } M^{-1}$; $\Delta S^\ddagger = -3 \text{ cal } M^{-1} K^{-1}$) are very similar to the corresponding parameters determined by Birus et al.⁶⁴ for desferriferrioxamine B ($\Delta H^\ddagger = 11.7 \text{ kcal } M^{-1}$; $\Delta S^\ddagger = -8 \text{ cal } M^{-1} K^{-1}$) and in excellent agreement with the data available⁸² for the water exchange process of $Fe(OH)^{2+}$ ($\Delta H^\ddagger = 10.1 \text{ kcal } M^{-1}$; $\Delta S^\ddagger = 1.3 \text{ cal } M^{-1} K^{-1}$). Cavasino and Di Dio⁸³ have examined the activation parameters related to $Fe(OH)^{2+}$ and various ligands (hydroxamic acids,^{66,76,77,84} catechols,⁸⁵ hydrocarboxylic acids⁸⁶) and found a narrow range of ΔH^\ddagger ($4.7 < \Delta H^\ddagger < 10.0 \text{ kcal } M^{-1}$) and consistently negative ΔS^\ddagger values ($-26 \text{ cal } M^{-1} K^{-1} < \Delta S^\ddagger < -5 \text{ cal } M^{-1} K^{-1}$).

Our kinetic results compared to literature data are in favor of a dissociative Eigen–Wilkins⁷⁸ mechanism for the reaction of $Fe(OH)^{2+}$ with pyoverdine PaA. The similarity between the rate constant determined for $Fe(OH)^{2+}$ with pyoverdine PaA and that obtained for hydroxamic acid⁶⁵ suggests that the formation rate limiting step of the ferric pyoverdine PaA complexes could be attributed to the coordination at hydroxamate site.

The dimer species $Fe_2(OH)_2^{4+}$ was found to be one order of magnitude more reactive than $Fe(OH)^{2+}$ (Table 9). The bimolecular rate constant k_3 measured for pyoverdine PaA is

about five times higher than that determined for acetohydroxamic acid⁷⁷ (Table 9). The little data reported in the literature for the reactivity of $Fe_2(OH)_2^{4+}$ with various ligands (catechols,⁸⁷ squaric acid,⁸⁸ tiron,^{88,89} dihydroxybiphenyl derivatives⁹⁰) show that the ligand influences the kinetic results, the rate constants values varying in a large range between $5 \times 10^2 M^{-1} s^{-1}$ and $5 \times 10^5 M^{-1} s^{-1}$ (Table 9).

The dissociation mechanism of the ferric pyoverdine PaA complexes (LFe , $LHFe^+$ and LH_2Fe^{2+}) in acidic conditions is illustrated in Figure 10. A step by step dissociation mechanism of the coordination sites has been found.

The first two steps involving two protons lead to the formation of an intermediate kinetic species I_2 (Table 6). Taking into account the absorption of the hydroxyquinoline moiety ($\epsilon_{403} \approx 800 M^{-1} cm^{-1}$), its extinction coefficient ($\epsilon_{403} = 2100 M^{-1} cm^{-1}$) is compatible, within large experimental errors, with that of the thermodynamically stable diprotonated ferrioxamine B⁶⁴ ($\epsilon_{426} \approx 1500 M^{-1} cm^{-1}$). Moreover, stopped-flow spectrophotometry at 560 nm verified that the hydroxyquinoline iron charge transfer band was no longer observed after the first two steps. The rate constant related to the second step $k_2 = 1.8 \times 10^3 M^{-1} s^{-1}$ is about one order of magnitude higher than the rate constant, attributed by Birus et al.,⁶⁴ to the dissociation of the first ferrioxamine B hydroxamate ($3.8 \times 10^2 M^{-1} s^{-1}$). This result might illustrate faster iron dissociation steps from catecholate-type coordination sites than from hydroxamate sites, as previously reported.⁹¹ All kinetic and spectrophotometric results are in favor of the loss of the hydroxyquinoline type bidentate coordination site during the two faster steps of the dissociation mechanism.

The rate constant $k_3 = (7.5 \pm 0.5) 10^{-2} M^{-1} s^{-1}$ determined for the third step (Table 6) is in good agreement with that determined by Birus et al.⁶⁴ for the acidic dissociation of the dihydroxamate species of ferrioxamine B ($(2.3 \pm 0.2) \times 10^{-2} M^{-1} s^{-1}$). The thermodynamic constant $K_{I_3} = 8 \pm 4 M^{-1}$ value is similar to those determined for the ferric dihydroxamate-ferric monohydroxamate equilibria of ferrioxamine B⁶⁴ ($2.0 M^{-1}$) and of acetohydroxamic complexes⁶⁵ ($1.2 M^{-1}$). The extinction coefficient of the intermediate species I_3 at 403 nm ($\epsilon_{I_3} = 1400 \pm 200 M^{-1} cm^{-1}$) can be favorably compared with that of the ferrioxamine B monohydroxamate intermediate⁶⁴ ($\epsilon_{426} = 1221 M^{-1} cm^{-1}$). By comparing our results to literature data the third step of our mechanism was attributed to the dissociation of the first pyoverdine PaA hydroxamate coordination site.

In agreement with previous dissociation kinetic studies carried out on ferrioxamine B and monohydroxamate ferric complexes,^{64,66,67} we propose two dissociation pathways for the final step of the ferric pyoverdine PaA complex: one proton dependent step leading to the release of Fe^{3+} , and one, proton independent step, liberating $Fe(OH)^{2+}$ (Figure 10).

The Fe^{3+} release pathway gave a thermodynamic constant $K_{Fe} = (1.4 \pm 0.6) \times 10^{-4}$ or a ratio of the rate constants $k_4/k_{-4} = (5 \pm 3) \times 10^{-5}$ which is similar to the corresponding value determined for the final dissociation step of ferrioxamine B⁶⁴ ($(8 \pm 3) \times 10^{-5}$). The rate constant $k_4 = (3.2 \pm 0.6) \times 10^{-4} M^{-1} s^{-1}$ determined for pyoverdine PaA is comparable to that obtained for ferrioxamine B ($(5 \pm 1) \times 10^{-4} M^{-1} s^{-1}$) by Birus et al.⁶⁴ The comparison between siderophore monohydroxamate

(81) Swaddle, T. W.; Merbach, A. E. *Inorg. Chem.* **1981**, *20*, 4212–4216.(82) Grant, M.; Jordan, R. B. *Inorg. Chem.* **1981**, *20*, 55–60.(83) Cavasino, F. P.; Di Dio, E. *J. Chem. Soc. A* **1970**, 1151–1154.(84) Fish, L. L.; Crumbliss, A. L. *Inorg. Chem.* **1985**, *24*, 2198–2204.(85) Mentasti, E.; Pelizzetti, E. *J. Chem. Soc., Dalton Trans.* **1973**, 2605–2608.(86) Mentasti, E. *Inorg. Chem.* **1979**, *18*, 1512–1515.(87) Xu, J.; Jordan, R. B. *Inorg. Chem.* **1988**, *27*, 1502–1507.(88) Sisley, M. J.; Jordan, R. B. *Inorg. Chem.* **1991**, *30*, 2190–2195.(89) Jordan, R. B.; Xu, J. H. *Pure Appl. Chem.* **1988**, *60*, 1205–1208.(90) Serratrice, G.; Zeghli, A.; Beghin, C. G.; Baret, P.; Pierre, J. L. *New J. Chem.* **1993**, *17*, 297–307.(91) Crumbliss, A. L. *Coord. Chem. Rev.* **1990**, *105*, 155–179.(92) Carrano, C. J.; Cooper, S. R.; Raymond, K. N. *J. Am. Chem. Soc.* **1979**, *101*, 599–604.

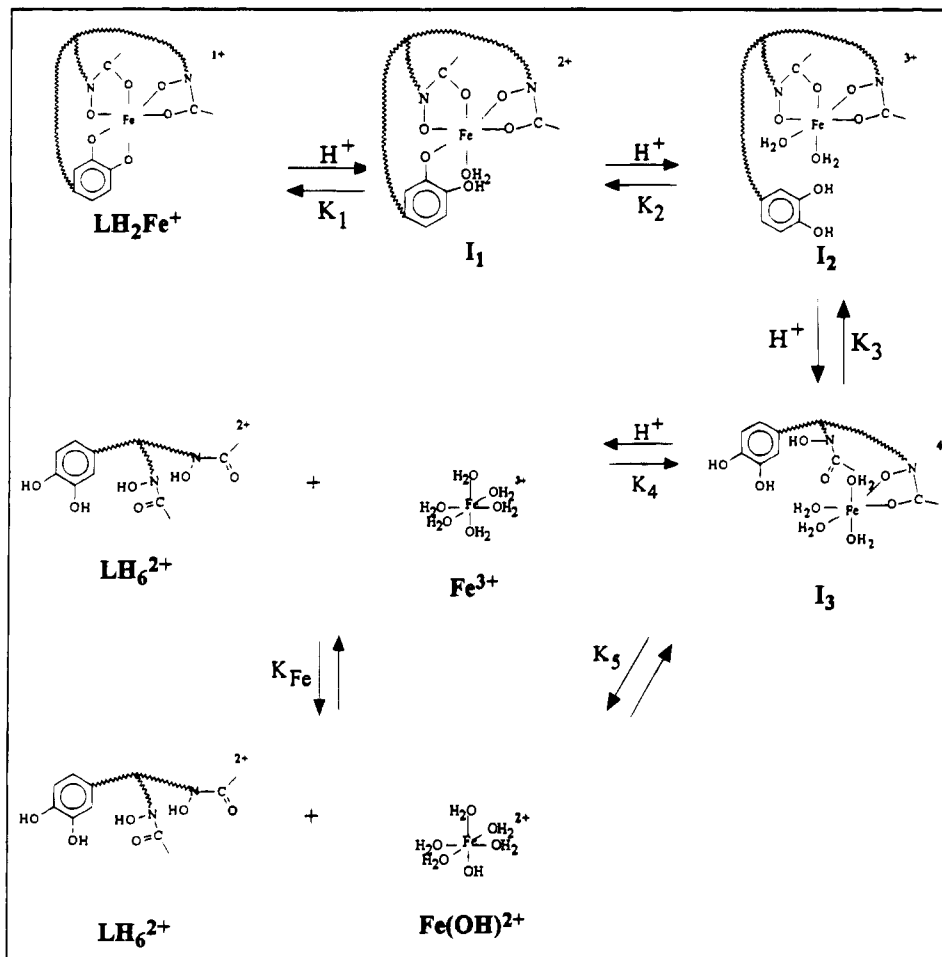
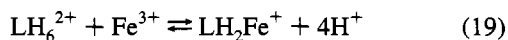


Figure 10. Formation and dissociation mechanism of ferric pyoverdin PaA complexes.

intermediates and monohydroxamate ferric complexes appears to be less satisfactory. Bimolecular protons attack on acetomonohydroxamate and *N*-methylacetomonohydroxamate ferric complexes gives rate constants ($6 \times 10^{-2} \text{ M}^{-1} \text{ s}^{-1}$ and $2.8 \times 10^{-3} \text{ M}^{-1} \text{ s}^{-1}$),⁶⁵ respectively, which are about two orders of magnitude higher than those determined for siderophores. Different steric hindrance, electronic and solvation effects could be important features which slow down the final step of Fe^{3+} release for siderophores compared to simple hydroxamic acids.

The proton independent final step takes into account the participation of an intramolecular proton. The corresponding first-order rate constant k_5 could not be determined with accuracy, but the order of magnitude of the rate constant k_{-5} related to the bimolecular reaction between $\text{Fe}(\text{OH})^{2+}$ and pyoverdin PaA ($k_{-5} \approx 10^3 \text{ M}^{-1} \text{ s}^{-1}$) is in agreement with $k'_2 = 7.7 \times 10^3 \text{ M}^{-1} \text{ s}^{-1}$ determined by the formation kinetic study of the pyoverdin PaA ferric complexes.

Finally, using the thermodynamic constants K_{I_1} , K_{I_2} , K_{I_3} , and K_{Fe} (Table 6) which were determined for the dissociation mechanism of the pyoverdin PaA ferric complexes, we were able to calculate the thermodynamic constant $K_{\text{LH}_2\text{Fe}} = 9 \times 10^{-3} \text{ M}^3$ related to the equilibrium:



The excellent agreement between this result and the same determination from our thermodynamic data $K_{\text{LH}_2\text{Fe}} = 7.9 \times 10^{-3} \text{ M}^3$ presented earlier in this paper confirms the validity of the proposed mechanism.

Pyoverdin PaA shows like the linear trihydroxamate siderophore, ferrioxamine B, a step by step dissociation mechanism, in spite of its "anchored structure" (Figure 1). The fast formation in acidic conditions of dihydroxamate kinetic intermediates shows the predominant role of the protons in decreasing the stability of the thermodynamic complexes and in creating more suitable species for an iron(III) transport mechanism. According to the microreversibility principle, the initial formation step of the ferric pyoverdin PaA corresponds to the final dissociation step involving the terminal hydroxamate coordination site. This step will be followed by faster folding processes of the flexible siderophore around the ferric cation (Figure 10).

In conclusion, our results have shown that pyoverdin PaA, like desferrioxamine B, is a strong and selective iron(III) chelator. The thermodynamic stability of these two ligands is not due to their rigidity, but to the nature of their coordination sites. These properties provide fast formation mechanisms and a reduction potential which is accessible to physiological reductants. Our complete physico-chemical study of iron pyoverdin PaA coordination properties has pointed out important features of a biological transport mechanism, a fast and selective uptake of iron(III) and the efficient participation to the release mechanism inside the cell of more labile protonated or ferrous pyoverdin PaA species.

Supplementary Material Available: Rate constants (Tables S1 and S2) and reduction potentials (Table S3) (3 pages). Ordering information is given on any current masthead page.